Published OnlineFirst September 15, 2017; DOI: 10.1158/0008-5472.CAN-17-0064

Microenvironment and Immunology

Cancer Research

# Tenascin-C and Integrin α9 Mediate Interactions of Prostate Cancer with the Bone Microenvironment

Rebeca San Martin[1], Ravi Pathak[2], Antrix Jain[1], Sung Yun Jung[3], Susan G. Hilsenbeck[4], María C. Piña-Barba[5], Andrew G. Sikora[2], Kenneth J. Pienta[6], and David R. Rowley[1]

## Abstract

Deposition of the extracellular matrix protein tenascin-C is part of the reactive stroma response, which has a critical role in prostate cancer progression. Here, we report that tenascin C is expressed in the bone endosteum and is associated with formation of prostate bone metastases. Metastatic cells cultured on osteo-mimetic surfaces coated with tenascin C exhibited enhanced adhesion and colony formation as mediated by integrin α9β1. In addition, metastatic cells preferentially migrated and colonized tenascin-C–coated trabecular bone xenografts in a novel system that employed chorioallantoic membranes of fertilized chicken eggs as host. Overall, our studies deepen knowledge about reactive stroma responses in the bone endosteum that accompany prostate cancer metastasis to trabecular bone, with potential implications to therapeutically target this process in patients. *Cancer Res; 77(21); 5977–88.* ©*2017 AACR.*

## Introduction

Local prostate cancer that progresses and invades outside the gland preferentially metastasizes to bone among other tissues (1). The formation of new micrometastases and the subsequent growth of macroscopic tumors results in bone pain and potentially pathologic fracture. These metastases are primarily osteoblastic. The specific mechanisms that promote metastasis to bone are not understood; however, the role of the microenvironment in bone has been proposed as an important player in this process (1). Specifically, the mechanisms that mediate colonization of prostate cancer cells to the bone endosteum and then promote colony expansion are essentially unknown; however, alterations in adhesion have been shown to affect metastatic potential (2). The bone endosteum is a layer of cells lining the internal trabecular bone and is composed of osteoprogenitor stem cells, resting and active osteoblasts, and osteoclasts. The endosteum is the site of the osteoblastic niche in bone, which has been shown to be important for hematopoietic stem cells self-renewal (3). Importantly, this same endosteal osteoblastic niche has been shown to be the site of prostate cancer metastases, and data suggest that prostate cancer cells compete with hematopoietic stem cells for this niche (4).

Tenascin-C is a hexameric extracellular matrix protein that is evolutionary conserved in the order *Chordata* (5) and plays an essential role in the development of bone and the nervous system (6, 7). Interestingly, the expression of tenascin-C in adult, differentiated tissues at homeostasis is negligible, but its deposition is essential for wound repair (8–10). Importantly, tenascin-C is expressed at sites of new bone deposition by osteoblasts (11). During bone development, tenascin-C was found in osteogenic cells that invade cartilage during endochondral ossification and in the condensed osteogenic mesenchyme that form new bone during intramembranous ossification and around new bone spicules. These studies also showed that after bone formation, some tenascin C remains located in the endosteum surface; however, it is not found in the mature bone matrix (12). Important to the results of the current study, elevated tenascin-C deposition is observed at sites of bone repair after fractures (13).

In prostate cancer, tenascin-C is deposited early during cancer progression and is a key hallmark of reactive stroma (14). Reactive stroma recapitulates a normal wound repair (15) and is composed of a heterogeneous population of vimentin-positive cancer-associated fibroblasts (CAF) and myofibroblasts, cells derived from tissue-resident mesenchymal stem cells (MSC) that express smooth muscle α actin and vimentin upon the influence of TGFβ (16). This tenascin-C enrichment of the tumor microenvironment affects cancer cell adhesion, migration, and proliferation (17). In this context, tenascin-C also exhibits immunosuppressive functions in tumors via regulation of cytokine/chemokine expression that affects inflammation and the immune landscape (18).

The reactive stroma response in prostate cancer initiates early in the disease, during prostatic intraepithelial neoplasia (19) and is predictive of biochemical recurrence after prostatectomy (20). Persistent deposition of tenascin-C by both CAFs and

[1]The Department of Molecular and Cellular Biology, Baylor College of Medicine, Houston, Texas. [2]Bobby R. Alford Department of Otolaryngology, Head and Neck Surgery, Baylor College of Medicine. Houston, Texas. [3]Department of Biochemistry and Molecular Biology, Baylor College of Medicine, Houston, Texas. [4]Breast Center, Dan L Duncan Comprehensive Cancer Center, Baylor College of Medicine, Houston, Texas. [5]Laboratorio de Biomateriales, Instituto de Investigaciones en Materiales, Universidad Nacional Autónoma de México, Mexico City, Mexico. [6]The James Buchanan Brady Urological Institute, Johns Hopkins University School of Medicine, Baltimore, Maryland.

**Note:** Supplementary data for this article are available at Cancer Research Online (http://cancerres.aacrjournals.org/).

**Corresponding Author:** David R. Rowley, Baylor College of Medicine, One Baylor Plaza, Houston, TX 77030. Phone: 713-798-6220; Fax: 713-790-1275; E-mail: drowley@bcm.edu

**doi:** 10.1158/0008-5472.CAN-17-0064

Published OnlineFirst September 15, 2017; DOI: 10.1158/0008-5472.CAN-17-0064



myofibroblasts (21) may foster the progression of prostate cancer and initiation of metastasis via differential adhesion patterns and transient EMT induction (22).

In the case of prostate cancer, metastases preferentially target bone (23). Following Paget's "seed and soil" hypothesis (24), the colonization of a secondary site by a cancer cell that has successfully escaped the primary tumor site is dependent on a suitable environment amenable to colonization. Therefore, the possibility arises that metastatic colonization initiates a reactive response at the secondary site (25), and/or an underlying pathology at the secondary site created a "fertile soil" in which the metastatic foci preferentially colonizes. Interestingly, the microenvironment changes present in prostate cancer bone metastases, in the context of a reactive tissue phenotype, have not been characterized.

We report here a spatial association of human prostate cancer bone metastases with reactive endosteum foci high in tenascin-C deposition and dissect the role of tenascin-C in regulating adhesion and colony initiation. Selective adhesion and colony formation on bone/tenascin-C surfaces was mediated by integrin α9β1 in prostate cancer cells in novel human three-dimensional (3D) osteogenic organoids and in egg chorioallantoic membrane (CAM) metastasis models that use tenascin-C–coated, humanized, bovine trabecular bone cubes. This work extends our understanding of bone metastasis mechanisms in prostate cancer and identifies α9 integrin–tenascin-C interaction as a key mediator.

## Materials and Methods

### Bone metastasis tissue microarray

Human bone metastasis tissue microarrays were constructed from the rapid autopsy program at University of Michigan (Ann Arbor, MI). TMA#85 contains 63 bone metastases samples, six liver metastasis samples, three lung metastasis samples, and 12 prostate cancer samples, representing a total of 32 patients. Tissue samples from bone metastasis include 10 patients with bone marrow–associated lesions and 12 patients with trabeculae-associated metastatic foci (in triplicate). This array was analyzed via IHC for the reactive stroma markers tenascin-C, pro-collagen I, smooth muscle α actin, vimentin, and immune cell makers CD14 and CD68 (Supplementary Experimental Procedures, Supplementary Tables S1 and S2).

### *In vitro* MSC-derived 3D endosteal organoid model

Human adult MSCs (Lonza) growing in T75 cell culture flasks were trypsinized using standard protocols and washed twice with 10 mL of BFS media (Supplementary Experimental Procedures) by centrifugation (400 rpm, 3 minutes). The cell pellet was resuspended in BFS media to a concentration of $4 \times 10^5$ cells/300 μL or $8 \times 10^5$ cells/300 μL. Cell culture inserts (Millipore. Millicell-CM 12 mm) were prepared as suggested by the manufacturer, and each chamber was seeded with 300 μL of the cell suspension. After overnight incubation, once MSC spheroids were formed, the BFS media in both the inner and outer chambers were substituted with complete osteogenic media (R&D CCM007 supplemented with CCM008). Osteogenic organoids were cultured for 7, 14, and 21 days, with media changes every 2 days. Control organoids were kept in BFS media for the appropriate time points, with media changes every 2 days.

For cancer coculture experiments, the media inside the insert were substituted with 300 μL of cancer cell–specific media containing $4 \times 10^5$ cells (LNCaP, VCaP, or PC3), and the media outside each insert was replaced with 600 μL of the same media, as needed. Control organoids were exposed to cancer cell media alone. After 24 hours of incubation at 37°C, 5% $CO_2$, the media in the outside chamber were replaced with fresh media. Coculture samples were harvested after 48 hours and processed for histology and IHC (Supplementary Experimental Procedures; Supplementary Table S3)

### *In vitro* trabecular bone scaffold culture system

Nukbone (Biocriss S.A. de C.V.) bovine trabecular bone scaffolds, in either 200 to 500 μm particles or 0.5-cm cube were coated with human, full-length tenascin-C (Millipore cat. no. CC06) or BSA control, by immersion of the bone fragments into a 100 μg/mL solution of either protein for 7 days. Coating was confirmed by IHC (Supplementary Experimental Procedures). For *in vitro* adhesion and proliferation experiments, coated NukBone cubes were cultured with 250,000 VCaP cells in DMEM/F-12 1:1 (Invitrogen) containing 0.1% BSA, without antibiotics, using nonadhesive (CM) inserts as described before.

### Prostate cancer cell lines adhesion to tenascin-C

Tenascin-C coating was done according to published protocols (26), with modifications. Using a 0.5-mm cutting template (ICN cat no 4215), we scored circles on the outside of the bottom of the cell culture wells (Osteo Assay surface, 24-well plates. cat. no. 3987 Corning or Costar nontreated, 6-well plates). In the case of the 6-well plate, 3 circles per well were inscribed. These circles were used as guides for microscopical analysis of coated surfaces. For coating, a 3 μL drop of human, full-length purified tenascin-C (Millipore cat. no. CC06) at the appropriate concentration (0, 5, 10, 25, 50, 75, and 100 μg/mL), in PBS pH 7.4, was applied in the center of each of the circles and incubated 48 hours at 37°C, until the droplets dried out. BSA at the appropriate concentrations was coated as control. Tenascin-C coating was verified as follows: coated wells were incubated for 72 hours in DMEM/F-12 1:1 (Invitrogen) containing 0.1% BSA, without antibiotics at 37°C and 5% $CO_2$. Plates were then fixed with 4% paraformaldehyde for 20 minutes at room temperature, and tenascin-C was detected via immunocytochemistry (AP-Vector Blue, Supplementary Experimental Procedures).

Cells (VCaP, PC3, and LNCaP) were seeded at a density of $1 \times 10^5$ cells/cm$^2$ in their basal media (DMEM/F-12 1:1 or RPMI) containing 0.1% BSA, without antibiotics. Cells were allowed to adhere for 3 hours at 37°C and 5% $CO_2$ before washing all wells three times with warm media. For imaging of adherent cells, 15 micrographs at a ×10 magnification were acquired for each of the experimental conditions, making sure to image more than 90% of the coated areas; quantification was performed with the cell counter function in the ImageJ software (27).

### Neutralizing of integrin α9β1 activity

Integrin neutralization was done as according to published protocols (28). In brief, VCaP cells were incubated in DMEM/F-12 1:1 (Invitrogen) containing 0.1% BSA, supplemented with α9β1-neutralizing antibody, clone Y9A2 (BioLegend cat. no. 351603) or mouse isotype control (mouse IgG, Sigma-Aldrich cat. no. I5381), at a concentration of 10 μg/mL for 30 minutes on ice before being seeded onto the tenascin-C–coated surfaces at a density of $2.2 \times 10^5$ cells/cm$^2$. As described before, cells were allowed to adhere for 3 hours before washing the wells and quantification of adherent

Published OnlineFirst September 15, 2017; DOI: 10.1158/0008-5472.CAN-17-0064



cells. Knockdown of α9 expression via siRNA was conducted and verified as outlined in the Supplementary Experimental Procedures (Supplementary Table S4).

### CAM-humanized bovine bone integrated experimental system

This system used the CAM of the chicken egg as a host for a xenograft composed of the "humanized" NukBone in combination with an organoid consisting of a mixture of VCaP cells (prostate cancer metastatic cell line) and the prostate-derived MSC hpMSC19I (16). Briefly, 8-day-old pathogen-free embryonated eggs were prepared as described previously (29) to expose the CAM. A neoprene ring was installed on top of the exposed CAM to delimit the xenograft location, and 100 μL of attachment factor (Gibco) was added in the chamber and allowed to set. The trabecular bone cube, coated with human tenascin-C, is placed on top. The prostate cell line–derived organoid (Supplementary Experimental Procedures) was deposited on this surface as well, about 0.5 cm away from the bone scaffold. The egg was then placed in a humidity-controlled incubator at 37°C for 6 days. Xenograft-bearing eggs were then incubated on ice for 20 minutes to anesthetize the chick. Using a syringe equipped with an 18-gauge needle, 3 mL of ice cold 4% paraformaldehyde was carefully injected through the taped window, to prevent contamination and touching the CAM/sample, to overlay the fixative over the CAM. Eggs were incubated on ice for a total of 4 hours to euthanize the chicks. The CAM was then dissected out in bulk. Tissues were placed in a 4-cm glass-bottomed cell culture dish (MatTek P35G-0-20-C) containing 5 mL of cold 4% paraformaldehyde and incubated at 4°C overnight without shaking. Tissues were then washed with three changes of PBS (5 mL each) for 5 minutes. Samples were then decalcified, paraffin embedded, and sectioned (Supplementary Experimental Procedures), taking care of embedding the xenograft with the CAM in the most proximal side of the block. For analysis of metastatic colonization of the trabecular bone fragment, 120 serial sections were acquired from each block, at a nominal thickness of 5 μm, collecting two sections per slide for a total of 60 slides. One of every eight slides were then stained with hematoxylin and eosin (H&E). Following microscopic evaluation for epithelial pockets associated with the bone, adjacent sections were analyzed by IHC studies to verify epithelial origin (pan-cytokeratin), and markers of interest (human ITGA9). Number of foci per sample were counted on the basis of the following rubric: metastatic epithelial foci is defined as (i) a collection of cuboidal cells that form clusters on the surface of the trabecular bone or (ii) a layer of cuboidal cells, in direct contact with the trabecular surface. Layers and clusters of cells, as previously described, that associated with different trabeculae and were at least 200 μm apart were counted as two separate foci. Layers and clusters of cells that associate with blood-like cells that rest atop the bone fragment were not considered as foci.

*In ovo* experiments followed approved protocols from the Institutional Animal Care and Use Committee.

### Statistical analysis

Statistical analysis was carried out on Prism Software (GraphPad). Cell counts for adhesion experiments were analyzed using one-way ANOVA with Tukey multiple comparisons test (***, $P < 0.001$; *, $P < 0.05$). qRT-PCR analysis was analyzed by two-way ANOVA ($n = 3$; *, $P < 0.05$; **, $P < 0.01$; ***, $P < 0.001$). CAM-trabecular bone xenografts foci count data were analyzed using Student $t$ test with Welch correction (***, $P < 0.001$).

## Results

### Identification of a reactive endosteum phenotype in trabeculae-associated metastatic foci of human prostate cancer

To assess a reactive phenotype in the context of bone metastasis, a human prostate cancer bone metastasis tissue array (TMA85 array, 63 metastasis samples, University of Michigan) was evaluated using dual IHC protocols as follows: tenascin-C/vimentin, smooth muscle α-actin/vimentin, pro-collagen I/vimentin, as well as IHC for the immune markers CD14 and CD68 (Supplementary Experimental Procedures). Image analysis revealed the bone metastasis can be classified into two distinct groups: (i) metastatic foci associated directly with the trabecular bone surface and (ii) metastatic foci associated with a reactive marrow stroma but not on the bone surface. Foci on the bone surface were associated with elevated immunoreactivity for tenascin-C in the endosteum (Fig. 1A and B), whereas smooth muscle α-actin staining was negligible (Fig. 1C). Of the 15 patients with trabeculae-associated metastasis, 11 showed trabecular TNC deposition in at least two of the three samples present in the array (73%). Adjacent areas immunoreactive to pro-collagen I were observed in 69% of tenascin-C–positive foci (Fig. 1B), with varying degrees of staining intensity from absent (Supplementary Fig. S1A) to high (Supplementary Fig. S1B–S1D). We subsequently termed this the reactive endosteum phenotype. In contrast, bone marrow–associated metastatic foci were negative for tenascin-C and pro-collagen deposition and showed a substantial immunoreactivity to smooth muscle α-actin in associated blood vessels (Fig. 1C). Elevated staining intensities of CD14 (Supplementary Fig. S2A) and CD68 macrophages (Supplementary Fig. S2B) were also observed in trabeculae-associated metastasis, when compared with marrow-associated foci.

### Differentiation of MSCs in nonadhesive conditions produces 3D osteogenic organoids

To evaluate interactions of an activated endosteum and prostate cancer metastatic cell lines, a human 3D osteogenic organoid model was generated. At 7 days of osteogenic induction in nonadherent conditions, human MSCs generated spheroids that differentiated into hard, white, opalescent organoids. These organoids were apparently tethered to the sides of the cell culture insert by distinct, fibrous, and flexible tendrils (Fig. 2A). Histologic analysis of 3D organoids revealed that a central mass of cells was surrounded by a flat and compact layer of outer cells that were nearly identical to the endosteum layer associated with trabecular bone (Fig. 2A–H and E). These cells were positive for osteocalcin, alkaline phosphatase, and osteonectin (SPARC), confirming osteoblast differentiation (Fig. 2A). Interestingly, this layer was also positive for tenascin-C deposition (Fig. 2A). Immunoreactivity to smooth α actin, while present in control organoids, was negative in osteo-induced conditions (Supplementary Fig. S3A and S3B). Finally, control 3D organoids retain a soft, loosely aggregated structure (Supplementary Fig. S4A) with reduced viability as shown by TUNEL staining (Supplementary Fig. S4B) and IHC for cleaved caspase-3 (Supplementary Fig. S4C).

### Prostate cancer cell lines preferentially adhere to tenascin-C high foci in 3D osteogenic organoids

Under coculture conditions with the 3D osteogenic organoids, the prostate bone metastatic cell line VCaP exhibited selective attachment to foci high in tenascin-C high, localized primarily on

Published OnlineFirst September 15, 2017; DOI: 10.1158/0008-5472.CAN-17-0064



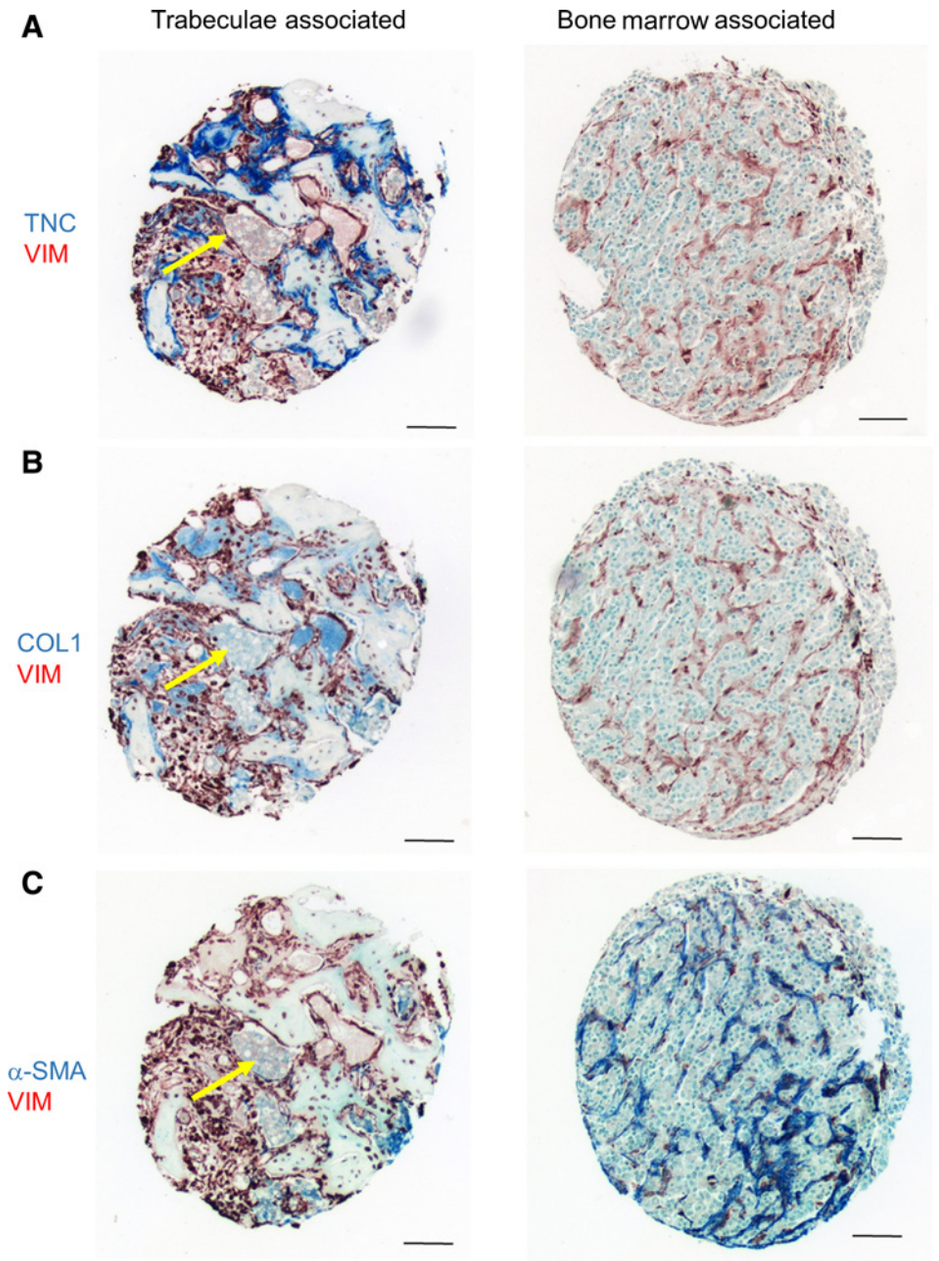


**Figure 1.**
Characterization of the reactive endosteum phenotype in prostate-derived bone metastasis. Bone metastasis tissue arrays were stained for reactive stroma markers. Characteristic trabeculae–associated and bone marrow metastasis samples are shown. Arrows, metastatic foci. Scale bar, 100 μm. **A,** Tenascin-C (AP-Vector Blue)-vimentin (HRP-Nova Red). **B,** Pro-collagen I (AP-Vector Blue)-vimentin (HRP-Nova Red). **C,** Smooth muscle α actin (AP-Vector Blue)-vimentin (HRP-Nova Red).

the endosteum tendrils (Fig. 2B). Distinct branching of the endosteal tendrils around the cancer clusters was observed in some samples. In stark contrast, coculture of the 3D organoids with the metastatic line PC-3, which is osteolytic, resulted degradation of the osteogenic organoid (Supplementary Fig. S5A) creating holes in the matrix, and detachment of the endosteum tendrils from the culture vessel wall. Endosteum tendrils that remained showed the characteristic tenascin-C enrichment with clusters of cancer cells. LNCaP prostate cancer cells (derived from a lymph node metastasis) adhered to the surface of 3D osteogenic organoids and elicited a reactive degradation response of the endosteum manifested as furrows in the underlying matrix (Supplementary Fig. S5B).

### Prostate cancer metastatic cells adhere to tenascin-C in a dose-dependent manner

To assess whether bone metastatic prostate cancer cell lines would adhere preferentially to tenascin-C, we used both non-treated, ultra-low adhesion cell culture plates and Osteo Assay plates (pretreated with osteo-mimetic calcium phosphate) that were coated with increasing concentrations of human tenascin-C. A stable coating with tenascin-C was verified via immunocytochemistry (Fig. 3A and B). At 3 hours of incubation in serum-free medium, we observed a differential and concentration-dependent adhesion of VCaP cells with an optimal adhesion observed with a coating of 75 μg/mL of tenascin-C (Fig. 3C). Furthermore, adhering VCaP cells proliferated and formed 3D foci at 72 hours of

Published OnlineFirst September 15, 2017; DOI: 10.1158/0008-5472.CAN-17-0064



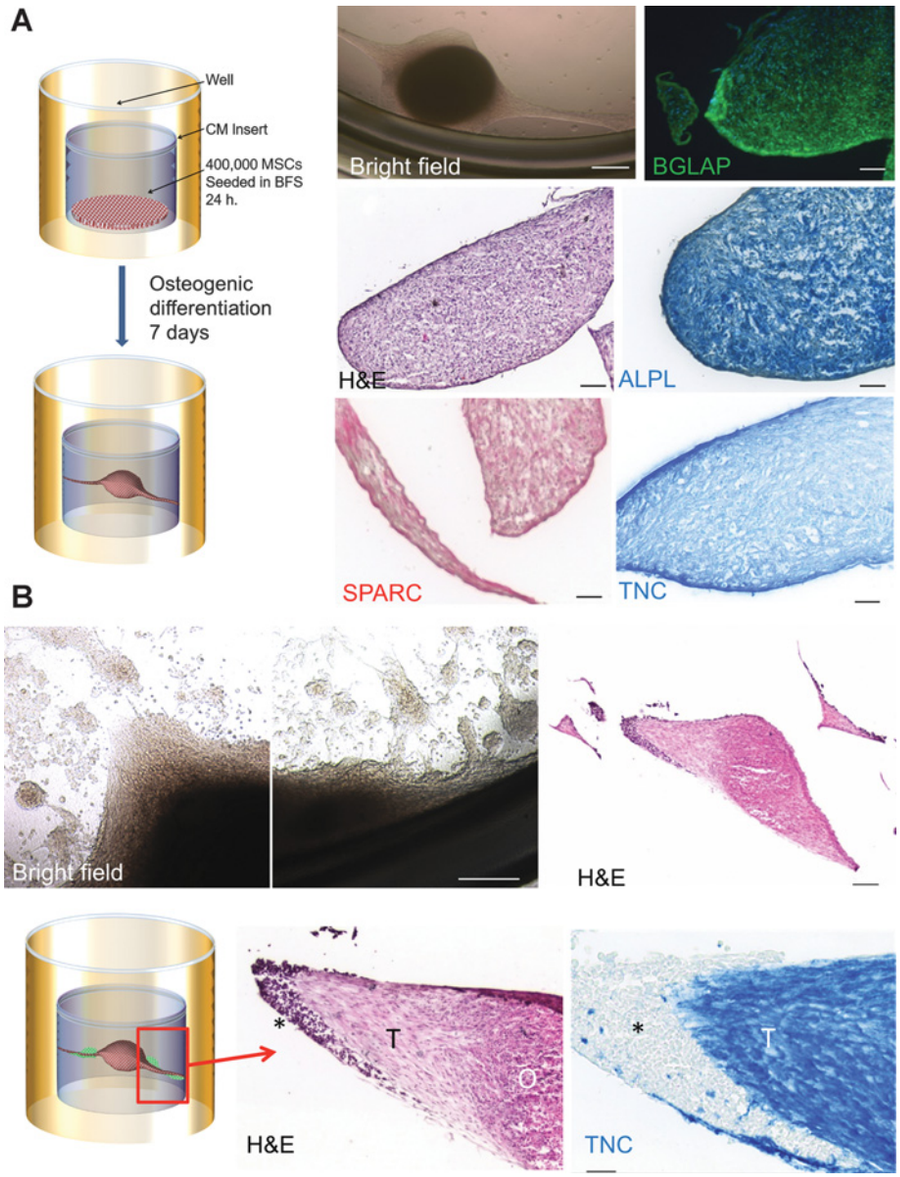


**Figure 2.**
MSC-derived osteogenic organoid and its interactions with the prostate cancer–derived metastatic cell line VCaP. A mesenchymal stem cell–derived osteogenic 3D spheroid model was developed to generate a fully defined, human model system where cancer and endosteum compartments are easily manipulated. **A,** Experimental protocol for organoid development. After 7 days of induction, organoids turn hard and opalescent, and develop endosteal tendrils. Brightfield image scale bar, 200 μm. The osteogenic organoid expresses osteoblast-specific markers: immunofluorescence, osteocalcin (BGLAP) FITC; DAPI, nuclear counterstain; H&E, IHC alkaline phosphatase (ALPL), osteonectin (SPARC), and tenascin-C (TNC). Scale bar, 100 μm. **B,** Coculture of the osteogenic organoid with the metastatic cell line VCaP. Cancer cells (*) associate at the sites of highest tenascin-C deposition, closer to the endosteal tendrils (T). Brightfield scale bar, 500 μm. H&E scale bar, 250 and 50 μm. IHC tenascin-C scale bar, 50 μm.

culture in serum-free media conditions (Fig. 3A; Supplementary Fig. S6A). Interestingly, the osteoclastic cell line PC3, and the lymph node–derived cell line LNCaP did not show enhanced adhesion to tenascin-C under these conditions (Supplementary Fig. S6B and S6C, respectively), and adhere to the substrate at significantly lower levels than VCaP (Supplementary Fig. S6D).

VCaP cells grown on tenascin-C–coated Osteo Assay plates adhere readily to the surface, showing spreading as early as 3 hours after seeding (Fig. 3B) and were also able to develop 3D foci at 72 hours of culture in serum-free conditions. Cells seeded on tenascin-C–coated osteo-mimetic plates adhere and initiate proliferation upon seeding, whereas control cultures exhibit a lag time of approximately 15 to 18 hours (Fig. 3D). Thereafter, both experimental and control cells proliferate at approximately the same rate. Cultures on tenascin-C plates also reach a higher population density compared with control, with both groups seeded in serum-free media (Fig. 3D). In addition, elevated population density was confirmed with VCaP cells seeded onto human tenascin-C–coated trabecular bone scaffolds (Nuk-Bone) as compared with control conditions in both serum free and low-serum culture conditions (Supplementary Figs. S7A and S7B, respectively) as shown via MTT assay (Supplementary Fig. S7C). These trabecular bone scaffolds (Supplementary Fig. S8A) readily absorb a stable coating of tenascin-C (Supplementary Fig. S8B). Finally, VCaP cells form 3D colonies on these tenascin-C–coated scaffolds in nonserum culture conditions (Supplementary Fig. S8C).

### Integrin α9β1 is essential for adhesion of prostate cancer–derived metastatic cells to tenascin-C

Owning to the rapid adhesion observed in both the low adhesion and osteo-mimetic, tenascin-C–coated cell culture conditions, we hypothesized that metastatic cell lines exhibited integrin profiles that mediated interaction with tenascin-C. Thus,

Published OnlineFirst September 15, 2017; DOI: 10.1158/0008-5472.CAN-17-0064



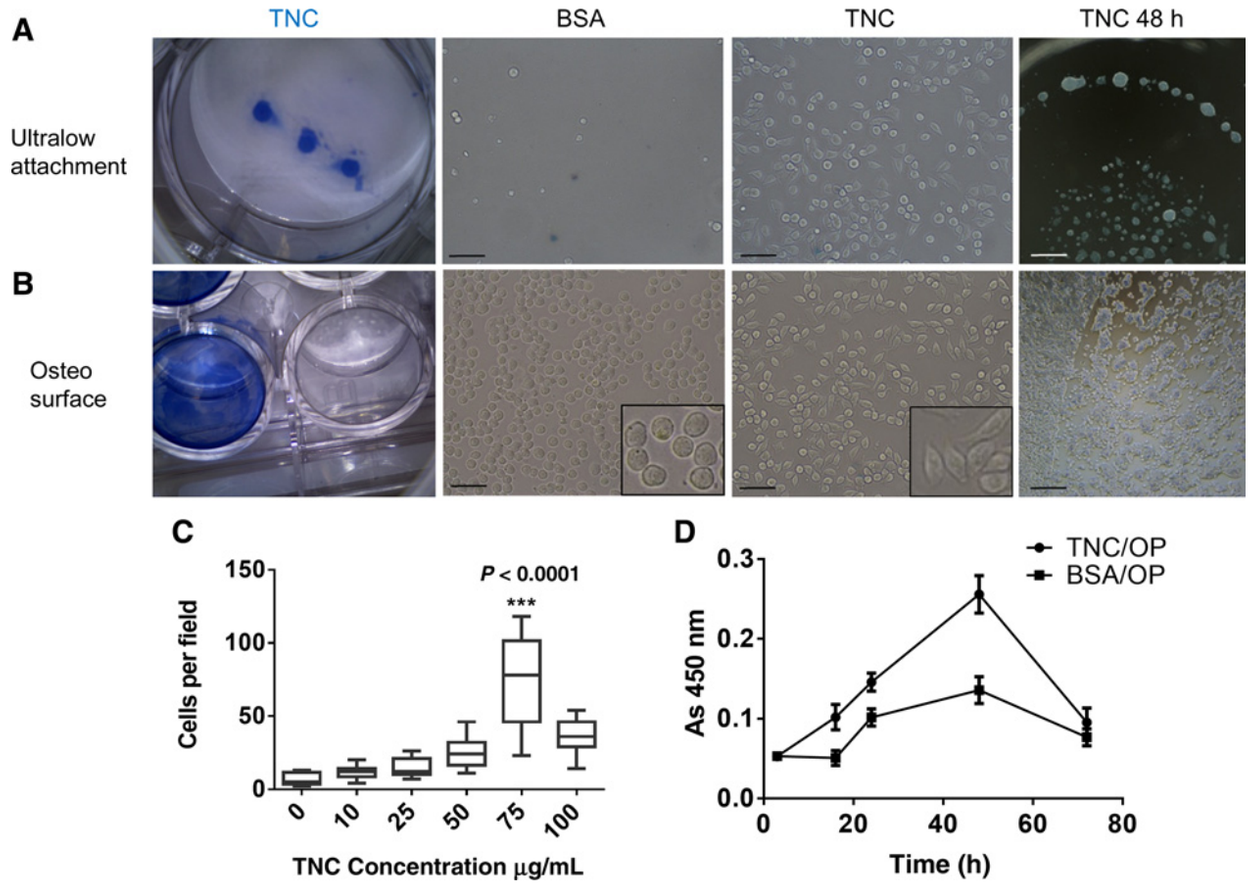


**Figure 3.**

VCaP adhesion and spreading in ultra-low attachment and osteo-mimetic plates is enhanced by tenascin-C coating. **A,** VCaP adhesion in ultra-low attachment plates. Confirmation of tenascin-C coating by immunocytochemistry (AP-Blue). VCaP attachment (3 hours) in tenascin-C or BSA control. Note that cells flatten out and spread on tenascin-C, and they do not lift from ULA plates after washing. Scale bar, 25 μm. **B,** VCaP adhesion in osteo-mimetic plates. Confirmation of tenascin-C coating by immunocytochemistry. VCaP attachment (3 hours) to tenascin-C. Scale bar, 25 μm. VCaP culture on tenascin-C–coated surfaces form 3D foci in nonserum-containing media at 48 hours regardless of culture surface type. Scale bar, 50 μm. **C,** VCaP attachment to tenascin-C is concentration dependent. Summary of three independent experiments analyzing cell number after 24-hour culture in osteo surfaces; data, mean values ± SEM. ***, $P < 0.001$. **D**, VCaP cells attach and initiate proliferation sooner on tenascin-C–coated osteo-mimetic plates and reach higher density relative to control (BSA-coated) conditions in serum-free media. Summary of four independent experiments analyzing cell proliferation on osteo surfaces via MTT assay; data, mean values ± SEM. $P < 0.0001$.

a cohort of prostate cell lines (PNT1A, BPH1, LNCaP, VCaP, PC3, 22RV1, Du145, and LNCaP C4-2B) was profiled for expression of integrins known to mediate tenascin-C binding. A relatively high expression level of α9 integrin was noted in VCaP cells (Fig. 4A; Supplementary Figs. S9 and S10), which was later confirmed via IHC for the α9β1 dimer in cells associated with 3D osteogenic organoids (Fig. 4B). Furthermore, IHC analysis showed cells immunoreactive to integrin α9 in 74% of the cancer foci associated with tenascin-C in the TMA85 tissue array samples (Fig. 4C). Finally, both neutralization of the α9β1 integrin dimer via neutralizing antibodies (Fig. 4D and E) and knockdown of the α9 subunit gene expression with siRNA (Fig. 4F and G; Supplementary Fig. S11A and S11B; Supplementary Table S5; and Supplementary Experimental Procedures) ablated VCaP adhesion to tenascin-C–coated osteo-mimetic surfaces. Together, these data support the hypothesis that the α9β1 integrin plays an important role in the adhesion and colonization of prostate cancer cells in the bone metastatic niche.

### Tenascin-C induces chemotaxis and colony formation of VCaP in a CAM-humanized bovine bone integrated experimental system

To model the interactions between reactive endosteum on trabecular bone and metastatic cancer cells, we developed an *in ovo* xenograft system in which a human tenascin-C–coated trabecular bovine cube was cocultured in close proximity to an organoid (Fig. 5A) comprised of bone metastatic cells (VCaP) and human prostate-derived MSCs (hpMSC 19-I) on a chicken egg CAM.

A mixture of VCAP and of hpMSC19I was cultured overnight under nonadhesive conditions to produce 3D organoids as we have reported previously (Supplementary Experimental Procedures; ref. 16). This mixture of cells starts contraction and segregation into distinct epithelial and stromal compartments as early as 3 hours after seeding (Fig. 5A, B, C). At this early time point, it is possible to detect the epithelial compartment via IHC for pan-cytokeratin and androgen receptor (Fig. 5D). These

Published OnlineFirst September 15, 2017; DOI: 10.1158/0008-5472.CAN-17-0064



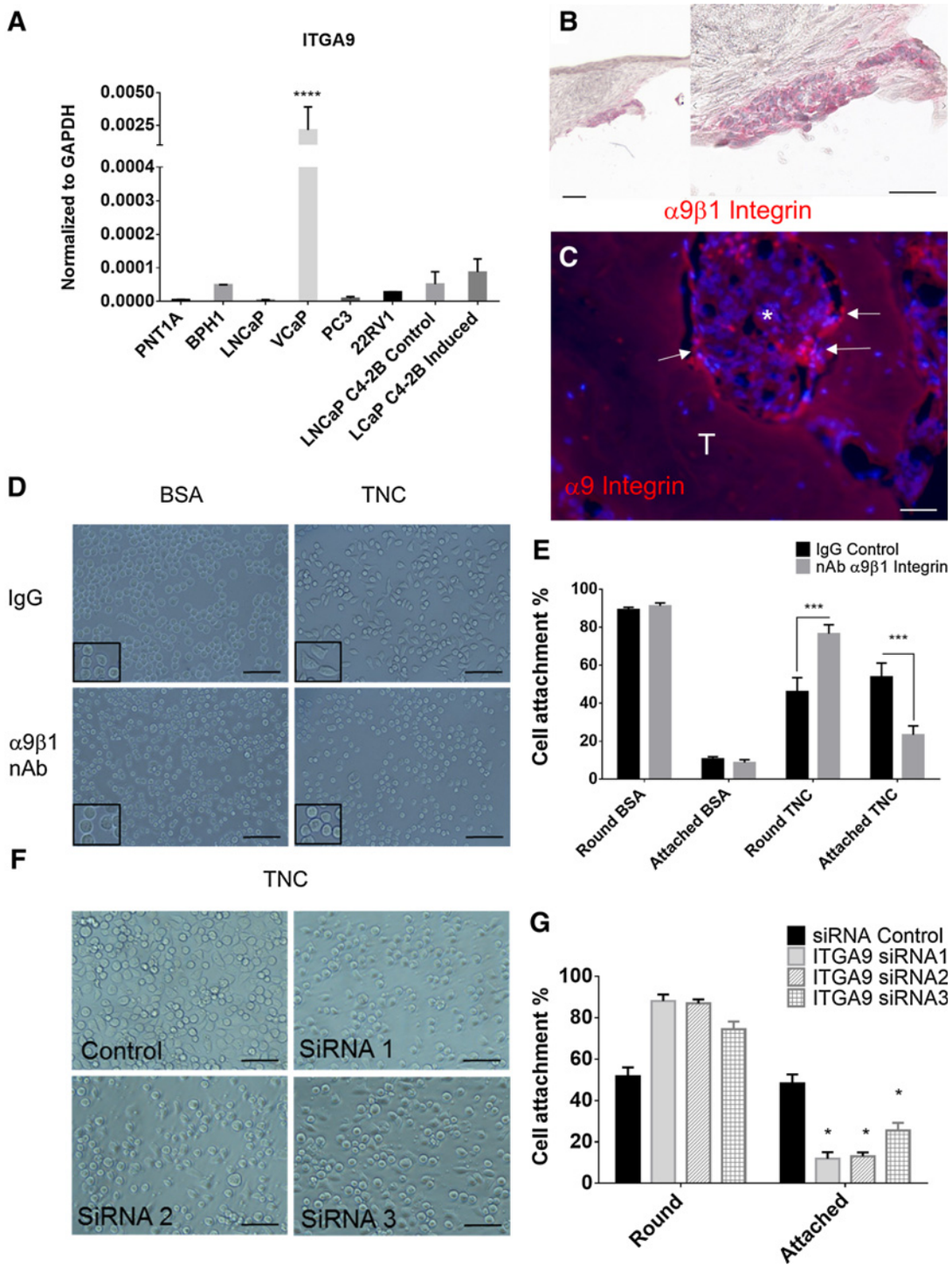


**Figure 4.**

VCaP adhesion to tenascin-C is mediated by α9β1 integrin. **A,** The metastatic prostate cell line VCaP expresses a significantly higher amount of integrin α9 when compared with other prostate cell lines. qRT-PCR data, mean values ± SEM; ****, $P < 0.0001$. **B,** Staining for the α9β1 integrin dimer in the osteogenic organoid coculture. Scale bar 100 μm. **C,** Staining for α9 integrin (Texas Red) in the human metastasis prostate array. Image shows an adjacent section to the sample shown in Fig. 1. Metastatic foci (*) shown associated with trabecular bone (T). Arrows, ITGA9 cells. Scale bar, 100 μm. **D,** Neutralization of α9β1 via a neutralizing antibody ablates attachment to tenascin-C in VCaP. **E,** Summary of three independent α9β1 neutralization experiments on tenascin-C–coated osteo surfaces; data, mean values ± SEM. ***, $P < 0.001$. **F,** Neutralization of α9 integrin via SiRNA ablates VCaP attachment to tenascin-C. **G,** Summary of three independent α9β1 knockdown-adhesion experiments on tenascin-C–coated osteo surfaces; data, mean values ± SEM.*, $P < 0.05$.

Published OnlineFirst September 15, 2017; DOI: 10.1158/0008-5472.CAN-17-0064



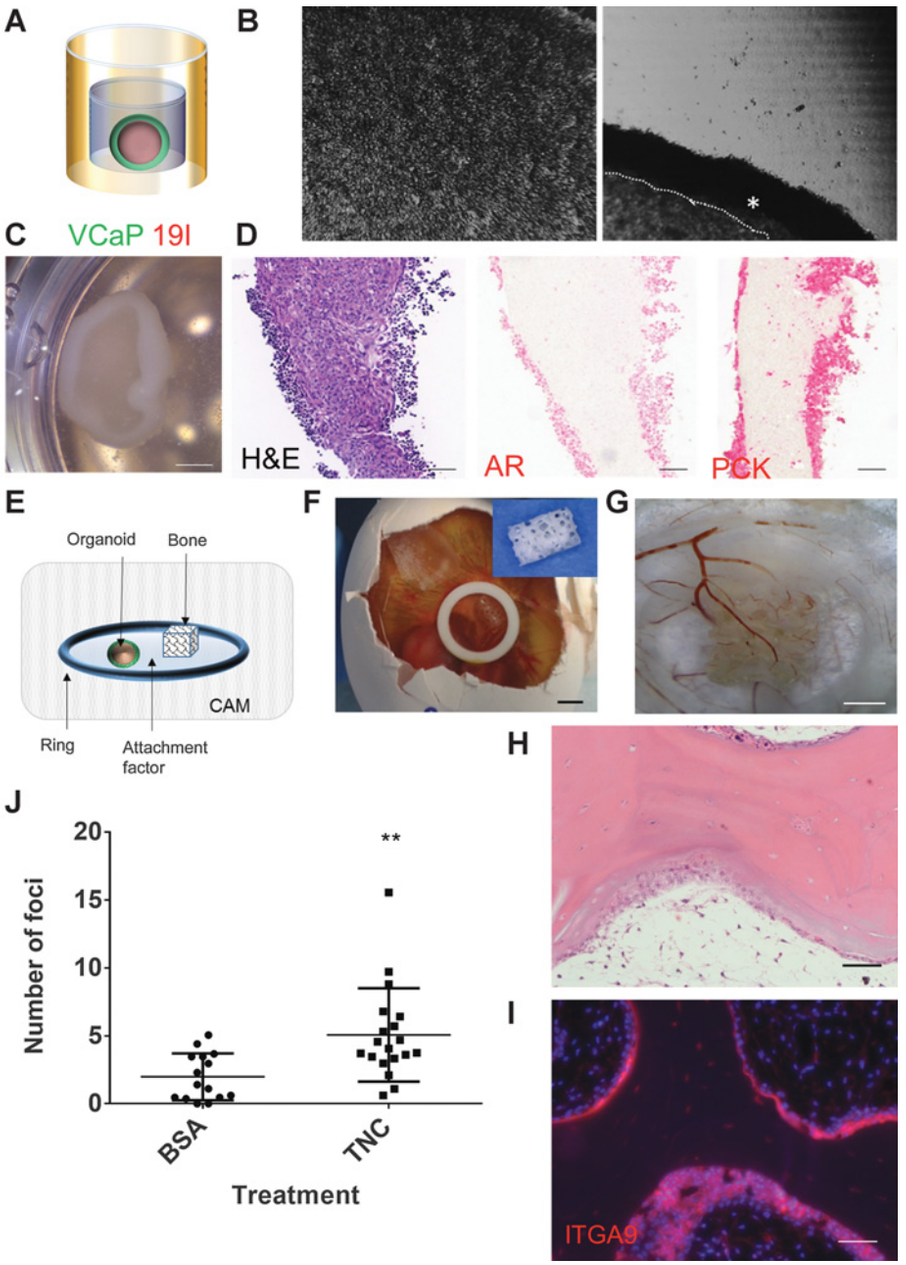


**Figure 5.**
The CAM-humanized bovine bone integrated experimental system shows preferential cancer cell chemotaxis and colonization bone scaffolds enriched in tenascin-C. **A,** Graphic representation of the prostate epithelial–stroma organoid structure. Distinct hpMSC 19-I (stroma) internal compartment self-segregates from an epithelial mantle. **B,** Formation of the prostate epithelial–stroma organoid. A mixture of hpMSC 19-I and VCaP is seeded in suspension in nonadhesive conditions. Two hours after seeding, the organoid contracts and segregation of the epithelial (*) and the stromal compartments occurs (dotted line, stromal–epithelial border). Images captured with the CytoSmart Live Cell Imaging System (Lonza). **C,** Brightfield image of the organoid at 24-hour incubation. Scale bar, 500 μm. **D,** Serial sections of the prostate organoid, H&E. IHC for androgen receptor (AR) and pan-cytokeratin (PCK) denote the epithelial compartment of the organoid. Scale bar, 100 μm. **E,** Experimental setup of the *in ovo* xenograft system. **F,** Trabecular bone scaffold *in ovo*. Inset, trabecular bone scaffold. Scale bar, 5 mm. **G,** Bulk dissection of the xenograft. Tenascin-C–coated bone xenograft after 6 days of incubation *in ovo*. The bone fragment associates with the CAM. Blood vessels infiltrate the trabecular bone xenograft. Scale bar, 2.5 mm. **H** and **I,** Serial sections of CAM-associated bone xenograft is colonized by VCaP. H&E, immunofluorescent α9 integrin (Texas Red); tissue counterstained with DAPI Scale bar, 100 μm. **J,** Summary of eight independent experiments (19 tenascin C samples, 15 control). Analyzing the number of VCaP foci associated with bone xenografts shows preferential recruitment to tenascin-C–coated scaffolds. ***, $P < 0.001$.

3D organoids were placed on the CAM of the fertilized chicken egg, along with Nukbone bovine trabecular bone cubes coated with either tenascin-C or BSA as control, as described previously (Fig. 5E and F).

After 6 days of *in ovo* incubation, trabecular bone cubes recruited CAM blood vessels that infiltrate into the trabecular bone cube in a tenascin-C–independent manner (Fig. 5G). Tenascin-C–coated trabecular bone cubes show colonization of VCaP cells, identified by expression of human α9 integrin, indicating these cells migrated from the organoid toward to scaffold (Fig. 5H and I). Quantification of foci revealed that VCaP preferentially migrate to tenascin-C–coated bone fragments as compared with BSA-coated controls (Fig. 5J).

### Tenascin-C elicits the production of collagen XIIa1 in metastatic prostate cells

To assess potential downstream effectors of tenascin-C–induced biology, two-dimensional RP/LC-MS analysis in VCaP cells cultured on tenascin-C–coated Osteo Assay plates was conducted (Supplementary Experimental Procedures). An increase in production of laminin subunit β2 (LAMB2), optineurin (OPTN), Golgi-associated, gamma adaptin ear containing, ARF binding protein 1 (GGA1), phospholipase D family member 3 (PLD3), and palmitoyl-protein thioesterase 2 (PPT2) was observed (Fig. 6A). Of relevance, a distinct increase (30-fold) of collagen12, α1 (COL12A1) protein was noted and subsequently confirmed in VCaP grown on 3D osteogenic organoids using

Published OnlineFirst September 15, 2017; DOI: 10.1158/0008-5472.CAN-17-0064



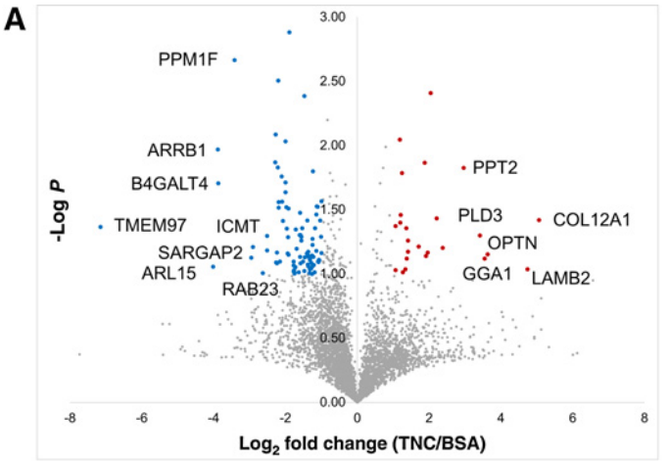


| Gene ID | Gene symbol | $Log_2$ fold |
|---|---|---|
| 1303 | COL12A1 | 5.06 |
| 3913 | LAMB2 | 4.73 |
| 10133 | OPTN | 3.63 |
| 26088 | GGA1 | 3.55 |
| 23646 | PLD3 | 3.42 |
| 9374 | PPT2 | 2.96 |
| 51715 | RAB23 | -2.64 |
| 23463 | ICMT | -2.90 |
| 23380 | SRGAP2 | -2.95 |
| 9647 | PPM1F | -3.42 |
| 8702 | B4GALT4 | -3.87 |
| 408 | ARRB1 | -3.89 |
| 54622 | ARL15 | -4.02 |
| 27346 | TMEM97 | -7.15 |

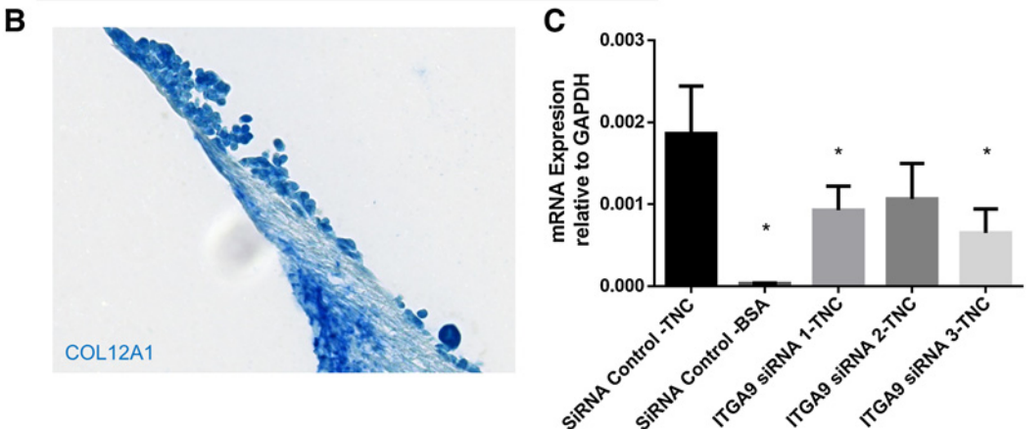


**Figure 6.**

Differential protein expression in VCaP cultured in tenascin-C-osteo plate. **A,** Mass spectrometry reveals enhanced expression of collagen 12A and laminin β2 subunit in VCaP because of culture on tenascin-C–coated osteo surfaces. **B,** VCaP that associate with the osteogenic organoid express COL12A1. IHC COL12A1 (blue). Methyl green, counterstain. **C,** Ablation of adhesion via integrin α9 knock out decreases expression of COL12A1 in VCaP when cells are cultured on tenascin-C–coated osteo-mimetic surfaces. Summary of three independent RT-PCR studies on the expression of COL12A1 upon ITGA9 knockout. *, $P < 0.05$

IHC (Fig. 6B). Ablation of adhesion to tenascin-coated osteo plates via siRNA knockdown of integrin α9 resulted in a decrease of transcript for COL12A1 in VCaP cells cultured on tenascin-C–coated osteo-mimetic surfaces (Fig. 6C), suggesting a direct link between cell binding and this osteogenic collagen production by the epithelial cell.

## Discussion

We report a reactive endosteum phenotype that accompanies trabecular bone–associated prostate cancer metastasis, characterized by elevated deposition of tenascin-C and collagen I. Although its expression is limited in adult differentiated bone, tenascin-C plays an essential role in bone repair processes, such as the formation of granulation tissue during fracture repair, in osteogenic differentiation, mineralization, and bone remodeling due to mechanical load (13, 30, 31). Furthermore, bone stromal cells and osteoblasts show increased tenascin-c expression upon *in vitro* coculture with prostate cancer–derived cell lines (32), suggesting that tenascin-c deposition could arise as a response to metastatic colonization. It has been previously suggested that prostate metastatic cells compete with hematopoietic stem cells for their niche in bone (33), a niche that has been shown to be enriched in tenascin-C during activation (34). Our studies show that bone metastatic prostate cancer cells differentially adhere, proliferate more rapidly, and form 3D colonies in tenascin-C–coated osteo-mimetic surfaces. Furthermore, in a 3D osteogenic organoid model, prostate cancer cells preferentially attach at sites high in tenascin-C *in vitro* and tenascin-C–coated bone fragments show enhanced metastatic colonization in an *in ovo* xenograft approach.

It is also important to note that the interaction of integrins with tenascin-C is mediated through the IDG and RGD sequences within the third fibronectin type III repeat in human tenascin-C (35). Of interest, the fibronectin type III repeat of mouse tenascin-C lacks the IDG and RGD sequences (35). It is possible that lack of these sequences in mouse tenascin-C may explain, in part, why transgenic mouse models of cancer rarely metastasize to bone or why injection of human cancer cells in immunocompromised mice rarely metastasize to bone. In contrast, studies where human fetal bone fragments were implanted into SCID mice showed preferential metastasis of tail vein–injected human

Published OnlineFirst September 15, 2017; DOI: 10.1158/0008-5472.CAN-17-0064



prostate cancer cells to human bone fragments as compared with implanted mouse bone or endogenous mouse skeleton (36). In light of our results, this is not surprising, as tenascin-C expression is high in fetal human bone (11, 12).

Repetitive bone loading in normal life leads to microscopic cracks or microfractures in bone that undergoes subsequent bone repair processes. In humans, these microfractures increase with age in an exponential manner (37). Tenascin-C is overexpressed in endosteum undergoing bone repair (13). In many cancer foci, we observed elevated tenascin-C deposition in the endosteum of the trabeculae represented in the section, not just in the immediate region occupied by foci of cancer cells. It is possible that prostate cancer cells preferentially colonize the tenascin-C high reactive endosteum of bone trabeculae that are undergoing the normal process of microfracture repair as a function of aging. In this scenario, data reported here might suggest that cancer cells may not induce the reactive endosteum; rather, an existing microfracture-associated reactive endosteum is a preferential site for seeding of metastatic cells and colony initiation/formation. As tenascin-C is highly deposited in the reactive stroma of primary prostate cancers (14), it is possible that cancer cells acquire a tenascin-C addiction prior to metastasis to bone.

It is estimated that 15% of the male population will develop invasive prostate cancer in the United States (38). In most cases, resection of the primary tumor and concomitant therapies grants a 15-year recurrence-free survival. Biochemical recurrence, as refers to elevated PSA levels, is usually the first sign of prostate cancer progression, which is followed by distant metastasis in about 5% of patients. Interestingly, distant metastasis occurs 8 to 10 years after biochemical recurrence (39). The mechanisms that mediate this delay in metastatic development are not understood. Evidence suggests that tumor cells disseminate from prostate cancer in as many as 25% of patients with localized disease and that higher concentrations of these cells in blood negatively correlate with survival (40). However, it has been proposed that disseminated cancer cells become dormant in the secondary site microenvironment through several mechanisms (41, 42). We propose that the tenascin-C–rich osteo environments used throughout our study model a normal age-related or androgen ablation–induced bone loss (43, 44) and/or subsequent incidence of subclinical microfractures. In this context, production of tenascin-C necessary for repair occurring at proximal site to a dormant foci might trigger their escape from dormancy, via differential cellular adhesion, consistent with previous findings (45).

Importantly, this study also provides evidence that metastatic prostate cancer cells interact with tenascin-C in the endosteum via the integrin α9β1 dimer (ITGA9 – ITGB1), as ablation of its activity via siRNA or neutralizing antibodies inhibits cell spreading on tenascin-C–coated osteo surfaces. Furthermore, integrin α9–positive cells are present at prostate metastatic foci enriched with tenascin-C in human samples (Fig. 5). Integrin α9β1 has been previously implicated in the induction of metastatic phenotypes in cancers where the primary tumor is also enriched in tenascin-C expression, such as breast (46–48), lung (49), and colon (50). Of key interest, α9β1 mediates the interaction between the hematopoietic stem cell and a tenascin-C–rich niche in the endosteum (34). Integrin α9β1 also plays a critical role in extravasation of neutrophils (51). Hence, the same integrin identified in the current study has been shown to mediate extravasation events and bone marrow colonization events in other normal cell types.

We also show here a significant induction in COL12A1 production by a prostate epithelial metastatic cell line (VCaP), which results from contact with tenascin-C on osteo-mimetic surfaces. Collagen XIIa (COL12A1) is a member of the fibril-associated collagens with interrupted triple helices (FACIT) family, where it contributes to the organization and mechanical properties of collagen fibrils (52). COL12A1 is present throughout mesenchymal tissues during development, but it is restricted to fascia and basement membranes in dermis, kidney, and muscle in adult organisms, a distribution that is conserved throughout vertebrate species (53). In bone development, a knockout mouse model for COL12A1 shows shorter, thinner long bones with low mechanical strength as well as decreased bone matrix deposition (54). COL12A-null osteoblasts differentiate slower with poor mineralization, showing abnormal polarization; a role in the establishment of cell–cell interactions during bone formation has been implicated (55). Given the predominantly osteoblastic nature of prostate cancer, it is enticing to hypothesize that tenascin-C induced production of COL12A1 in metastatic cells would stimulate osteoblast differentiation and osteoid deposition at metastatic sites.

In conclusion, given that the reactive microenvironment response is essential for prostate cancer progression, our work on characterizing the reactive response in the bone microenvironment and what effect it has on metastasis addresses a major gap in the field. Herein, we identify tenascin-C as an extracellular component of the osteoblastic niche that fosters the colonization and growth of trabecular-associated bone metastasis. *In vitro* and *in vivo* studies established that metastatic cells bearing integrin α9β1 selectively migrate and colonize bone enriched in tenascin-C, suggesting that therapies aimed at blocking this axis will positively impact the outcome for patients with metastatic prostate cancer.

## Disclosure of Potential Conflicts of Interest

No potential conflicts of interest were disclosed.

## Authors' Contributions

**Conception and design:** R. San Martin, K.J. Pienta, D.R. Rowley
**Development of methodology:** R. San Martin, R. Pathak, A.G. Sikora, D.R. Rowley
**Acquisition of data (provided animals, acquired and managed patients, provided facilities, etc.):** R. San Martin, R. Pathak, A. Jain, S.Y. Jung, D.R. Rowley
**Analysis and interpretation of data (e.g., statistical analysis, biostatistics, computational analysis):** R. San Martin, S.Y. Jung, S.G. Hilsenbeck, D.R. Rowley
**Writing, review, and/or revision of the manuscript:** R. San Martin, S.Y. Jung, S.G. Hilsenbeck, A.G. Sikora, K.J. Pienta, D.R. Rowley
**Administrative, technical, or material support (i.e., reporting or organizing data, constructing databases):** A. Jain, S.Y. Jung, M.C. Piña-Barba, D.R. Rowley
**Study supervision:** K.J. Pienta
**Other (performed experiments):** A. Jain

## Acknowledgments

We thank Truong Dang and William Bingman III for technical assistance.

## Grant Support

This work is funded by grants from CRPIT RP140616 (to D.R. Rowley), NIH NCI U01CA143055 (to D.R. Rowley and K.J. Pienta), R01CA58093 (to D.R. Rowley), the Caroline Weiss Law Endowment (to A.G. Sikora), the

CPRIT Proteomics and Metabolomics Core Facility Award RP12009, CCSG P30CA125123, and the Comprehensive Cancer Center Grant NIH NCI P30CA125123 (to Baylor College of Medicine).

The costs of publication of this article were defrayed in part by the payment of page charges. This article must therefore be hereby marked *advertisement* in accordance with 18 U.S.C. Section 1734 solely to indicate this fact.

Received January 7, 2017; revised June 2, 2017; accepted September 5, 2017; published OnlineFirst September 15, 2017.

## References

1. Jin JK, Dayyani F, Gallick GE. Steps in prostate cancer progression that lead to bone metastasis. Int J Cancer 2011;128:2545–61.
2. Lee YC, Bilen MA, Yu G, Lin SC, Huang CF, Ortiz A, et al. Inhibition of cell adhesion by a cadherin-11 antibody thwarts bone metastasis. Mol Cancer Res 2013;11:1401–11.
3. Calvi LM, Adams GB, Weibrecht KW, Weber JM, Olson DP, Knight MC, et al. Osteoblastic cells regulate the haematopoietic stem cell niche. Nature 2003;425:841–6.
4. Shiozawa Y, Pedersen EA, Havens AM, Jung Y, Mishra A, Joseph J, et al. Human prostate cancer metastases target the hematopoietic stem cell niche to establish footholds in mouse bone marrow. J Clin Invest 2011; 121:1298–312.
5. Tucker RP, Drabikowski K, Hess JF, Ferralli J, Chiquet-Ehrismann R, Adams JC. Phylogenetic analysis of the tenascin gene family: evidence of origin early in the chordate lineage. BMC Evol Biol 2006;6:60.
6. Mackie EJ, Murphy LI. The role of tenascin-C and related glycoproteins in early chondrogenesis. Microsc Res Tech 1998;43:102–10.
7. Chiquet-Ehrismann R, Mackie EJ, Pearson CA, Sakakura T. Tenascin: an extracellular matrix protein involved in tissue interactions during fetal development and oncogenesis. Cell 1986; 47:131–9.
8. Hakkinen L, Hildebrand HC, Berndt A, Kosmehl H, Larjava H. Immunolocalization of tenascin-C, alpha9 integrin subunit, and alphavbeta6 integrin during wound healing in human oral mucosa. J Histochem Cytochem 2000;48:985–98.
9. Okamura N, Hasegawa M, Nakoshi Y, Iino T, Sudo A, Imanaka-Yoshida K, et al. Deficiency of tenascin-C delays articular cartilage repair in mice. Osteoarthritis Cartilage 2010;18:839–48.
10. Mackie EJ, Halfter W, Liverani D. Induction of tenascin in healing wounds. J Cell Biol 1988;107:2757–67.
11. Mackie EJ, Abraham LA, Taylor SL, Tucker RP, Murphy LI. Regulation of tenascin-C expression in bone cells by transforming growth factor-beta. Bone 1998;22:301–7.
12. Mackie EJ, Thesleff I, Chiquet-Ehrismann R. Tenascin is associated with chondrogenic and osteogenic differentiation *in vivo* and promotes chondrogenesis *in vitro*. J Cell Biol 1987;105:2569–79.
13. Kilian O, Dahse R, Alt V, Zardi L, Hentschel J, Schnettler R, et al. mRNA expression and protein distribution of fibronectin splice variants and high-molecular weight tenascin-C in different phases of human fracture healing. Calcified Tissue Int 2008;83:101–11.
14. Tuxhorn JA, Ayala GE, Smith MJ, Smith VC, Dang TD, Rowley DR. Reactive stroma in human prostate cancer: induction of myofibroblast phenotype and extracellular matrix remodeling. Clin Cancer Res 2002;8:2912–23.
15. Desmouliere A, Chaponnier C, Gabbiani G. Tissue repair, contraction, and the myofibroblast. Wound Repair Regen 2005;13:7–12.
16. Kim W, Barron DA, San Martin R, Chan KS, Tran LL, Yang F, et al. RUNX1 is essential for mesenchymal stem cell proliferation and myofibroblast differentiation. Proc Natl Acad Sci U S A 2014;111:16389–94.
17. Midwood KS, Orend G. The role of tenascin-C in tissue injury and tumorigenesis. J Cell Commun Signal 2009;3:287–310.
18. Jachetti E, Caputo S, Mazzoleni S, Brambillasca CS, Parigi SM, Grioni M, et al. Tenascin-C Protects Cancer Stem-like Cells from Immune Surveillance by Arresting T-cell Activation. Cancer Res 2015;75:2095–108.
19. Tuxhorn JA, Ayala GE, Rowley DR. Reactive stroma in prostate cancer progression. J Urol 2001;166:2472–83.
20. Ayala GE, Tuxhorn JA, Wheeler TM, Frolov A, Scardino PT, Ohori M, et al. Reactive stroma as a predictor of biochemical free recurrence in prostate cancer. Clin Cancer Res 2003;9:4792–801.
21. Schauer IG, Ressler SJ, Tuxhorn JA, Dang TD, Rowley DR. Elevated epithelial expression of interleukin-8 correlates with myofibroblast reactive stroma in benign prostatic hyperplasia. Urology 2008;72:205–13.
22. Huang W, Chiquet-Ehrismann R, Moyano JV, Garcia-Pardo A, Orend G. Interference of tenascin-C with syndecan-4 binding to fibronectin blocks cell adhesion and stimulates tumor cell proliferation. Cancer Res 2001;61:8586–94.
23. Bubendorf L, Schopfer A, Wagner U, Sauter G, Moch H, Willi N, et al. Metastatic patterns of prostate cancer: an autopsy study of 1,589 patients. Hum Pathol 2000;31:578–83.
24. Paget S. The distribution of secondary growths in cancer of the breast. 1889. Cancer Metast Rev 1989;8:98–101.
25. Bonfil RD, Chinni S, Fridman R, Kim HR, Cher ML. Proteases, growth factors, chemokines, and the microenvironment in prostate cancer bone metastasis. Urologic Oncol 2007;25:407–11.
26. Probstmeier R, Pesheva P. Tenascin-C inhibits beta1 integrin-dependent cell adhesion and neurite outgrowth on fibronectin by a disialoganglioside-mediated signaling mechanism. Glycobiology 1999; 9:101–14.
27. Schneider CA, Rasband WS, Eliceiri KW. NIH Image to ImageJ: 25 years of image analysis. Nat Methods 2012;9:671–5.
28. Taooka Y, Chen J, Yednock T, Sheppard D. The integrin alpha9beta1 mediates adhesion to activated endothelial cells and transendothelial neutrophil migration through interaction with vascular cell adhesion molecule-1. J Cell Biol 1999;145:413–20.
29. Li M, Pathak RR, Lopez-Rivera E, Friedman SL, Aguirre-Ghiso JA, Sikora AG. The *in ovo* chick chorioallantoic membrane (CAM) assay as an efficient xenograft model of hepatocellular carcinoma. J Vis Exp 2015 Oct 9;(104). doi: 10.3791/52411.
30. Morgan JM, Wong A, Yellowley CE, Genetos DC. Regulation of tenascin expression in bone. J Cell Biochem 2011;112:3354–63.
31. Webb CM, Zaman G, Mosley JR, Tucker RP, Lanyon LE, Mackie EJ. Expression of tenascin-C in bones responding to mechanical load. J Bone Miner Res 1997;12:52–8.
32. Sung SY, Hsieh CL, Law A, Zhau HE, Pathak S, Multani AS, et al. Coevolution of prostate cancer and bone stroma in three-dimensional coculture: implications for cancer growth and metastasis. Cancer Res 2008;68: 9996–10003.
33. Yu C, Shiozawa Y, Taichman RS, McCauley LK, Pienta K, Keller E. Prostate cancer and parasitism of the bone hematopoietic stem cell niche. Crit Rev Eukaryot Gene Expr 2012;22:131–48.
34. Nakamura-Ishizu A, Okuno Y, Omatsu Y, Okabe K, Morimoto J, Uede T, et al. Extracellular matrix protein tenascin-C is required in the bone marrow microenvironment primed for hematopoietic regeneration. Blood 2012; 119:5429–37.
35. Adams JC, Chiquet-Ehrismann R, Tucker RP. The evolution of tenascins and fibronectin. Cell Adh Migr 2015;9:22–33.
36. Nemeth JA, Harb JF, Barroso U Jr, He Z, Grignon DJ, Cher ML. Severe combined immunodeficient-hu model of human prostate cancer metastasis to human bone. Cancer Res 1999;59:1987–93.
37. Schaffler MB, Choi K, Milgrom C. Aging and matrix microdamage accumulation in human compact bone. Bone 1995;17:521–25.
38. Siegel RL, Miller KD, Jemal A. Cancer statistics, 2015. CA Cancer J Clin 2015;65:5–29.
39. Boorjian SA, Thompson RH, Tollefson MK, Rangel LJ, Bergstralh EJ, Blute ML, et al. Long-term risk of clinical progression after biochemical recurrence following radical prostatectomy: the impact of time from surgery to recurrence. Eur Urol 2011;59:893–9.
40. Danila DC, Heller G, Gignac GA, Gonzalez-Espinoza R, Anand A, Tanaka E, et al. Circulating tumor cell number and prognosis in progressive castration-resistant prostate cancer. Clin Cancer Res 2007;13:7053–8.
41. van der Toom EE, Verdone JE, Pienta KJ. Disseminated tumor cells and dormancy in prostate cancer metastasis. Curr Opin Biotechnol 2016;40: 9–15.

Published OnlineFirst September 15, 2017; DOI: 10.1158/0008-5472.CAN-17-0064




42. Shiozawa Y, Berry JE, Eber MR, Jung Y, Yumoto K, Cackowski FC, et al. The marrow niche controls the cancer stem cell phenotype of disseminated prostate cancer. Oncotarget 2016;7:41217–32.
43. Mittan D, Lee S, Miller E, Perez RC, Basler JW, Bruder JM. Bone loss following hypogonadism in men with prostate cancer treated with GnRH analogs. J Clin Endocrinol Metab 2002;87:3656–61.
44. Greenspan SL, Coates P, Sereika SM, Nelson JB, Trump DL, Resnick NM. Bone loss after initiation of androgen deprivation therapy in patients with prostate cancer. J Clin Endocrinol Metab 2005;90:6410–7.
45. Ruppender N, Larson S, Lakely B, Kollath L, Brown L, Coleman I, et al. Cellular Adhesion Promotes Prostate Cancer Cells Escape from Dormancy. PLoS One 2015;10:e0130565.
46. Ota D, Kanayama M, Matsui Y, Ito K, Maeda N, Kutomi G, et al. Tumor-alpha9beta1 integrin-mediated signaling induces breast cancer growth and lymphatic metastasis via the recruitment of cancer-associated fibroblasts. J Mol Med 2014;92:1271–81.
47. Ioachim E, Charchanti A, Briasoulis E, Karavasilis V, Tsanou H, Arvanitis DL, et al. Immunohistochemical expression of extracellular matrix components tenascin, fibronectin, collagen type IV and laminin in breast cancer: their prognostic value and role in tumour invasion and progression. Eur J Cancer 2002;38:2362–70.
48. Oskarsson T, Acharyya S, Zhang XH, Vanharanta S, Tavazoie SF, Morris PG, et al. Breast cancer cells produce tenascin C as a metastatic niche component to colonize the lungs. Nat Med 2011;17:867–74.
49. Sun X, Fa P, Cui Z, Xia Y, Sun L, Li Z, et al. The EDA-containing cellular fibronectin induces epithelial-mesenchymal transition in lung cancer cells through integrin alpha9beta1-mediated activation of PI3-K/AKT and Erk1/2. Carcinogenesis 2014;35:184–91.
50. Gulubova M, Vlaykova T. Immunohistochemical assessment of fibronectin and tenascin and their integrin receptors alpha5beta1 and alpha9beta1 in gastric and colorectal cancers with lymph node and liver metastases. Acta Histochem 2006;108:25–35.
51. Mambole A, Bigot S, Baruch D, Lesavre P, Halbwachs-Mecarelli L. Human neutrophil integrin alpha9beta1: up-regulation by cell activation and synergy with beta2 integrins during adhesion to endothelium under flow. J Leukoc Biol 2010;88:321–7.
52. Chiquet M, Birk DE, Bonnemann CG, Koch M. Collagen XII: Protecting bone and muscle integrity by organizing collagen fibrils. Int J Biochem Cell Biol 2014;53:51–4.
53. Bader HL, Keene DR, Charvet B, Veit G, Driever W, Koch M, et al. Zebrafish collagen XII is present in embryonic connective tissue sheaths (fascia) and basement membranes. Matrix Biol 2009;28:32–43.
54. Izu Y, Ezura Y, Koch M, Birk DE, Noda M. Collagens VI and XII form complexes mediating osteoblast interactions during osteogenesis. Cell Tissue Res 2016;364:623–35.
55. Izu Y, Sun M, Zwolanek D, Veit G, Williams V, Cha B, et al. Type XII collagen regulates osteoblast polarity and communication during bone formation. J Cell Biol 2011;193:1115–30.

Cancer Research
The Journal of Cancer Research (1916–1930) | The American Journal of Cancer (1931–1940)

AACR American Association for Cancer Research

# Tenascin-C and Integrin α9 Mediate Interactions of Prostate Cancer with the Bone Microenvironment

Rebeca San Martin, Ravi Pathak, Antrix Jain, et al.

*Cancer Res* 2017;77:5977-5988. Published OnlineFirst September 15, 2017.